A Magnetic Integrated Method Suppressing Power Fluctuation for EV Dynamic Wireless Charging System

Ke Shi, Chunsen Tang, *Member, IEEE*, Zhihui Wang, *Member, IEEE*, Xiaofei Li, *Member, IEEE*, Yuanzhao Zhou, and Yingjun Fei

***Abstract*—This article proposes a magnetic integrated method for the coupler of the electric vehicle dynamic wireless charging system to suppress power fluctuation by transforming the problem into designing a stable equivalent mutual inductance between the receiving coil and transmitting coils on the road. Both primary-side and secondary-side couplers adopt a magnetic integrated design. The primary-side coupler integrates a reverse coil inside the transmitting coil, and the secondary-side coupler integrates a coil in the *LCC* resonance compensation inside the receiving coil. Two advantages are unveiled through theoretical analysis of system characteristics: the original single mutual inductance is replaced by the mutual inductance difference between the two reverse series transmitting coils and the receiving coil to determine the power transmission, which suppresses output power fluctuation; the secondary-side integrated inductor coil replaces the external bulky compensation inductor in the *LCC* resonance compensation network and additionally realizes better zero-voltage switching conditions. The optimized design process considering the additional couplings is given based on circuit analysis. A prototype is implemented to validate the proposed design. Experimental results show that the output power fluctuation is within $\pm 4\%$ during dynamic charging at a power level of 4.5 kW, and the efficiency reaches 91.6%.**

***Index Terms*—Electric vehicle dynamic wireless charging (EVDWC), integrated magnetic coupler, power fluctuation suppression, reverse coil, short-individual structure.**

I. Introduction

ELECTRIC vehicle dynamic wireless charging (EVDWC) system realizes a continuous wireless power supply during the driving of the electric vehicle (EV). When the EV equipped with a receiving coil passes the road surface, the electric energy from the transmission line buried under the road surface is continuously transmitted to the battery through the air gap. Therefore, the EV can work continuously, which greatly improves its practicality and convenience. The EVDWC system provides effective solutions to problems such as the high cost of EV batteries [1], short cruising range [2], and potential safety hazards during charging [3]. In the EVDWC system, there are two common structures named long-track-loop structure and short-individual structure. The long-track-loop structure is constituted by a coil whose dimension in the EV-moving direction is much longer than the EV. Instead, the short-individual structure is composed of a series of coils with dimensions close to the EV. The EVDWC system with a short-individual structure itself only provides the transmitting coils coupled with the receiving coil. This feature helps to improve the efficiency of the EVDWC system and avoid electromagnetic field radiation from the noncoupled part [4]. It has a suitable coupling coefficient and is adaptable to supply multiple EVs simultaneously. Therefore, the short-individual structure is the ideal layout of the EVDWC system to adapt to future practical applications.

However, in the process of dynamic power transmission, the relative position between the transmitting coils in the segmented layout and the receiving coil will change, which results in a variation in the mutual inductance between them. The drop of mutual inductance will cause output power fluctuation [5]. The power fluctuation makes the EV unable to charge effectively in the drop area and may affect the battery life [6].

Based on previous research, the solution to power fluctuation in the EVDWC system with a short-individual structure is mainly studied from the following three aspects. The first one is to reduce the variation of the inherent coupling coefficient between the transmitting coil and the receiving coil by changing the shape of the main magnetic coupler [7]–[9]. The focuses of these methods are coil shape, arrangement, magnetic core structure, and winding method. The second one is to adopt control strategies or multiphase excitation [10]–[13]. In general, the feasibility of the proposed control strategies had been verified, but there are still two serious problems. One is that additional device sensors and controllers greatly increase the complexity of the EVDWC system. The other is that the fast-moving speed of the receiver in the EVDWC system makes the control strategy difficult to implement and apply. The third one is to optimize the tolerance of compensation network parameters or to design impedance matching circuits [14], [15]. Optimizing the compensation parameters had been proved to improve the stability of the EVDWC system output, but the effect is limited.

Manuscript received August 24, 2021; revised November 15, 2021; accepted January 7, 2022. Date of publication January 11, 2022; date of current version February 18, 2022. This work was supported in part by the National Natural Science Foundation of China under Grant 52007012 and in part by the Fundamental Research Funds for the Central Universities under Grant 2020CDJYGZDH005. Recommended for publication by Associate Editor O. C. Onar. *(Corresponding author: Chunsen Tang.)*

The authors are with the School of Automation, Chongqing University, Chongqing 400000, China (e-mail: foreversk@outlook.com; cstang@cqu.edu.cn; wangzhihui@cqu.edu.cn; xiaofei.li@cqu.edu.cn; 327708679@qq.com; 1934563798@qq.com).

Color versions of one or more figures in this article are available at https://doi.org/10.1109/TPEL.2022.3142021.

Digital Object Identifier 10.1109/TPEL.2022.3142021

In this article, a magnetic integrated method is presented to solve the output power fluctuation and further improve the performance in the EVDWC system. It is mainly reflected in two aspects. At the transmitter, the integrated reverse coil is used to suppress the power fluctuation. The reverse coil was proven to mitigate the mutual inductance variation against the charging distance [16]–[19] or misalignment [20]–[24] for statics inductive power transfer systems with a single transmitter and receiver. In this article, the integrated reverse coil is used to achieve the stable equivalent mutual inductance between the receiving coil and the transmitting coils on the road, to realize the suppression of power fluctuation in the EVDWC system. At the receiver, the compensation inductor in the *LCC* resonant topology is integrated to achieve the compactness of the coupler and realize the zero-voltage switching (ZVS) condition configuration. The use of coupled coils to achieve compensation inductors was studied in [25]–[27], and they focused on constructing new power transmission channels for optimizing the misalignment performance under specific conditions. Overall, compared with the power transfer mode using a single mutual inductance, the mutual inductance difference has more potential to achieve a stable power transmission. This article proposes a novel solution for the EVDWC system based on magnetic integration, with output power fluctuation suppression and a ZVS working condition configuration. Two design variables are introduced, one is mainly used to achieve power stabilization, and the other is mainly used to obtain the desired inverter output phase angle to ensure the ZVS working condition. The contributions of this article include the following.

1) A magnetic integration method is proposed, including the series reverse winding of the transmitting coil and the resonant compensation inductor at the secondary side. The tricky issue of suppressing power fluctuation during the transition process in the short-individual structure EVDWC system is solved, and the ZVS condition is optimized.
2) The problem of suppressing power fluctuation is transformed into designing a stable equivalent mutual inductance between the receiving coil and transmitting coils on the road. The expression between equivalent mutual inductance and output power is established, and the relationship between the coil parameters and the mutual inductance characteristics of the reverse coil at the transition position is derived. The careful design method of the integrated reverse coil is proposed.
3) The functional relationship between the input impedance phase angle and the mutual inductance produced by the integrated inductor coil and the transmitting coils is derived. The design method of the integrated inductor coil is proposed based on the expression, and better ZVS working conditions are realized.

The rest of this article is organized as follows. In Section II, a magnetic integrated method using integrated reverse coils and an integrated inductor coil is proposed. Based on circuit analysis, the output power characteristics and ZVS Analysis are studied and presented, respectively. In Section III, the optimized design process considering multiple magnetic couplings is presented.

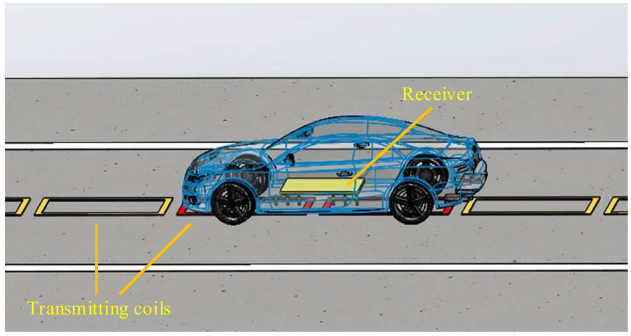

Fig. 1. EVDWC system with a short-individual structure.

In Section IV, the practical system is built and measured to verify the validity of the proposed method. Finally, Section V concludes this article.

II. System Configuration and Characteristics Analysis

A. System Configuration

The design of the transmitting coils in the EVDWC system with a short-individual structure is shown in Fig. 1. It is a layout method comprehensively considering the length of the EV and the energy utilization rate. Whenever the receiving coil reaches the center of a transmitting coil, the next coil is activated and the previous coil is disconnected. When the receiving coil moves along the track, the transmitting coils below the EV are activated and turned OFF in turn. In the working area accompanied by the EV, only the two transmitting coils are activated while the outer coils on both sides are not activated. This feature corresponds to its less energy waste and lower electromagnetic leakage characteristics. From a structural point of view, the analysis of two adjacent transmitting coils is sufficient for all working conditions and can verify the working principle of the proposed method.

The power fluctuation issue in the EVDWC system with a short-individual structure is essentially due to the variation of the mutual inductance between the transmitting coils and the receiving coil when EV moving. In this article, the coupling variation characteristics are changed by integrating new coupling coils at the transmitter with the original magnetic coupler unchanged. The coupling coils are added to obtain an equivalent mutual inductance difference to replace the original single coupling. At the receiver, a coupling coil is added to realize compensation inductance, introducing a design variable to obtain the desired inverter output phase angle to ensure the ZVS working condition. Without adding new components, the integrated design can not only suppress output power fluctuation effectively but also ensure a ZVS working condition.

The proposed integrated design for the EVDWC system with a short-individual structure is shown in Fig. 2. The coupler consists of three plates, including two identical transmitters and one receiver. The transmitter is constructed by a magnetic core board and two coils. The receiver is constructed by a magnetic core plate, a shield plate, and two coils. Among the

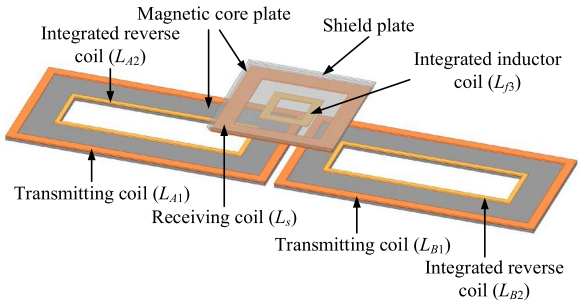

Fig. 2. Proposed magnetic coupler for the EVDWC system with a short-individual structure.

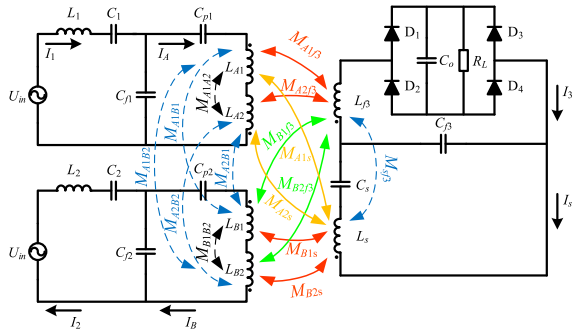

Fig. 3. Equivalent circuit topology of the EVDWC system with integrated design.

coils of the coupler, L_{A1} and L_{B1} are two transmitting coils. L_{A2} and L_{B2} are integrated reverse coils. L_s is the receiving coil. L_{sf3} is the inductor coil on the secondary-side *LCC* resonance compensation network.

B. Circuit Modeling

The double-sided *LCC* compensation topology was proven to be ideal for the EVDWC system [28], [29]. It possesses features that the resonant frequency is not affected by the coupling coefficient and load conditions with constant output current characteristics realized. The topology is a reasonable choice for the EVDWC system. In this article, the double-sided *LCC* topology is adopted to verify the proposed method.

Two coils are integrated into the magnetic coupler as compensation inductor and part of the transmitting coil, respectively. Therefore, the magnetic coupler possesses new characteristics due to the increased cross-couplings. The fundamental harmonic approximation (FHA) is adopted in this article.

The equivalent circuit topology of the EVDWC system with integrated design is shown in Fig. 3. U_{in} is the inverter ac output voltage. The variation in the output voltage during charging is a slow variable relative to the duty cycle. In the process of ac steady-state analysis, the output voltage can be considered to remain unchanged. Due to the constant output current characteristic, the load can be equivalent to a resistance R_L. The coils L_{A1} and L_{A2} are connected in reverse series as the first transmitter. The coils L_{B1} and L_{B2} are connected in reverse series as the second transmitter. The coils L_s and L_{f3} are integrated as the receiver. The addition coils and the main coils share the same ferrite and shielding plate. L_1 and L_2 are compensation inductors. C_1, C_2, C_{f1}, C_{f2}, C_{p1}, C_{p2}, C_s, and C_{f3} are compensation capacitors. C_o is the filter capacitor. There are fifteen significant coupling mutual inductances, M_{A1B2}, M_{A1B1}, M_{A2B2}, M_{A2B1}, M_{A1A2}, M_{B1B2}, M_{A1f3}, M_{A2f3}, M_{B1f3}, M_{B2f3}, M_{A1s}, M_{A2s}, M_{B1s}, M_{B2s}, and M_{sf3} in the system. Among them, M_{A1B2}, M_{A1B1}, M_{A2B2}, M_{A2B1}, M_{A1A2}, M_{B1B2} are the mutual inductances between two sets of primary-side transmitting coils. M_{A1f3}, M_{A2f3}, M_{B1f3}, M_{B2f3}, M_{A1s}, M_{A2s}, M_{B1s}, M_{B2s} are the mutual inductances between the secondary-side coils and primary-side transmitting coils. M_{sf3} is the mutual inductance between the receiving coil and the secondary-side compensate inductor coil. I_A and I_B are the currents of the transmitting coils, and I_s is the current of the receiving coil. I_1 and I_2 are the inverter output currents of two compensation networks, respectively. I_3 is the final output current. ω is the system operating frequency.

C. Output Power Calculation and ZVS Analysis

To be more concise and simplify the calculation process, the corresponding mutual inductances are defined as

$$\begin{aligned} M_{Af} &= M_{A1f3} - M_{A2f3} \\ M_{As} &= M_{A1s} - M_{A2s} \\ M_{Bf} &= M_{B1f3} - M_{B2f3} \\ M_{Bs} &= M_{B1s} - M_{B2s} \\ M_{AB} &= M_{A1B1} + M_{A2B2} - M_{A1B2} - M_{A2B1}. \end{aligned} \tag{1}$$

M_{A1A2}, M_{B1B2}, and M_{sf3} are the internal mutual inductances directly connected in series in the circuit, and they are also usually fixed. Therefore, they can be directly equivalent to the components in the circuit as follows:

$$\begin{aligned} L_A &= L_{A1} + L_{A2} - 1/(\omega^2 C_{p1}) - 2M_{A1A2} \\ L_B &= L_{B1} + L_{B2} - 1/(\omega^2 C_{p2}) - 2M_{B1B2} \\ L_{se} &= L_s - 1/(\omega^2 C_s) + M_{sf3} \\ L_{fe3} &= L_{f3} + M_{sf3} \\ C_{fe3} &= C_{f3}/(1 + \omega^2 M_{sf3} C_{f3}) \\ R_e &= 8R_L/\pi^2 \end{aligned} \tag{2}$$

Furthermore, the simplified circuit topology of the system is obtained based on the FHA method and Kirchhoff law, as shown in Fig. 4. The series connection of L_1 and C_1 is equivalent to L_{f1}, and the series connection of L_2 and C_2 is equivalent to L_{f2}. The magnetic couplings are represented by dependent sources. The power losses of the components are neglected to simplify the analysis.

The KCL equations are expressed as in (3).

The resonant relationship is expressed as

$$\begin{aligned} &\omega^2 L_{f1} C_{f1} = \omega^2 L_{f2} C_{f2} = \omega^2 (L_A + M_{AB}) C_{f1} \\ &= \omega^2 (L_B + M_{AB}) C_{f2} = \omega^2 L_{se} C_{fe3} = \omega^2 L_{fe3} C_{fe3} = 1. \end{aligned} \tag{4}$$

By substituting (4) into (3), it can be simplified as in (5).

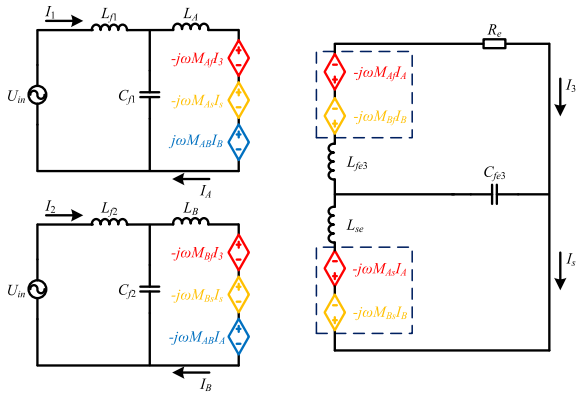

Fig. 4. Simplified circuit topology.

Therefore, the values of transmitting coil currents and output currents are calculated as

$$\begin{cases} \left|\dot{I}_A\right| = \frac{1}{\omega L_{f1}}\left|\dot{U}_{\text{in}}\right| \\ \left|\dot{I}_B\right| = \frac{1}{\omega L_{f2}}\left|\dot{U}_{\text{in}}\right| \\ \left|\dot{I}_3\right| = \frac{(L_{f1}M_{Bs}+L_{f2}M_{As})}{\omega L_{f1}L_{f2}L_{se}}\left|\dot{U}_{\text{in}}\right|. \end{cases} \tag{6}$$

Obviously, after the parameters are determined, the transmitting coil currents and output current only depend on the input voltage. The constant output current characteristics of the primary-side and secondary-side circuits are maintained.

To simplify calculations, based on the symmetry of the system parameters, the corresponding parameters are set as

$$L_{f1} = L_{f2} = L_f. \tag{7}$$

The system output power is expressed as

$$P_{\text{out}} = \left|\dot{I}_3\right|^2 R_e = K_1 {M_{ABs}}^2 \left|\dot{U}_{\text{in}}\right|^2 R_e \tag{8}$$

where $M_{ABs} = M_{As} + M_{Bs}, K_1 = 1/(\omega^2 {L_f}^2 {L_{se}}^2)$.

In the output power expression, K_1 is only related to the system parameter design and does not change during the EV moving. Due to the constant output current characteristics, U_{in} and R_e are also fixed parameters. Therefore, for the proposed EVDWC system with the magnetic integrated design, the output power fluctuation is only determined by the variation in the square of M_{ABs}. The result of mathematical derivation in (8) is compatible with the single coupling mode, and the essence of power transmission has not changed. It is tricky to smooth the mutual inductance used for power transmission in the traditional single coupling system. In this article, a smooth equivalent mutual inductance M_{ABs} can be obtained through the design of the magnetic coupler.

It is also necessary to analyze the system resonance state under the addition of multiple couplings. The total inverter output current calculated by (5) is expressed as

$$\dot{I}_{\text{in}} = \dot{I}_1 + \dot{I}_2 = \frac{(R_e M_{ABs} - 2j\omega M_{ABf} L_{se}) M_{ABs} \dot{U}_{\text{in}}}{\omega^2 {L_f}^2 {L_{se}}^2} \tag{9}$$

where $M_{ABf} = M_{Af} + M_{Bf}$.

Z_{in} represents the input impedance of the entire system. Z_{in} is expressed as

$$Z_{\text{in}} = \frac{\dot{U}_{\text{in}}}{\dot{I}_{\text{in}}} = \frac{j\omega^2 {L_f}^2 {L_{se}}^2}{M_{ABs}(jR_e M_{ABs} + 2\omega L_{se} M_{ABf})}. \tag{10}$$

The phase angle between the inverter output voltage and current is expressed as α, which can reflect the resonance state of the system. The positive and negative values of α represent the inductive and capacitive, respectively. In addition, its absolute value represents the degree to which the system deviates from the resonance point. The tangent of α is expressed as

$$\tan\alpha = \frac{\text{Im}(Z_{\text{in}})}{\text{Re}(Z_{\text{in}})} = \frac{2\omega L_{se} M_{ABf}}{R_e M_{ABs}}. \tag{11}$$

According to (11), even under reasonable parameter configuration, the system will not completely work at the theoretical resonance point. Therefore, the ratio of M_{ABf} to M_{ABs} can be designed to be small, which can ensure the system normal working state and the ZVS working condition.

According to (8) and (11), the output power fluctuation suppression and the parameters design of the ZVS working condition can realize based on the design optimization of the two design variables of M_{ABs} and M_{ABf}. To suppress the output power fluctuation, the primary-side integrated reverse coils

$$\begin{bmatrix} j\omega L_{f1} + \frac{1}{j\omega C_{f1}} & -\frac{1}{j\omega C_{f1}} & 0 & 0 & 0 & 0 \\ -\frac{1}{j\omega C_{f1}} & j\omega L_A + \frac{1}{j\omega C_{f1}} & 0 & j\omega M_{AB} & -j\omega M_{As} & -j\omega M_{Af} \\ 0 & 0 & j\omega L_{f2} + \frac{1}{j\omega C_{f2}} & -\frac{1}{j\omega C_{f2}} & 0 & 0 \\ 0 & j\omega M_{AB} & -\frac{1}{j\omega C_{f2}} & j\omega L_B + \frac{1}{j\omega C_{f2}} & -j\omega M_{Bs} & -j\omega M_{Bf} \\ 0 & -j\omega M_{As} & 0 & -j\omega M_{Bs} & j\omega L_{se} + \frac{1}{j\omega C_{fe3}} & -\frac{1}{j\omega C_{fe3}} \\ 0 & -j\omega M_{Af} & 0 & -j\omega M_{Bf} & -\frac{1}{j\omega C_{fe3}} & j\omega L_{fe3} + \frac{1}{j\omega C_{fe3}} + R_e \end{bmatrix}$$

$$\cdot \begin{bmatrix} \dot{I}_1 \\ \dot{I}_A \\ \dot{I}_2 \\ \dot{I}_B \\ \dot{I}_s \\ \dot{I}_3 \end{bmatrix} = \begin{bmatrix} \dot{U}_{\text{in}} \\ 0 \\ \dot{U}_{\text{in}} \\ 0 \\ 0 \\ 0 \end{bmatrix} \tag{3}$$

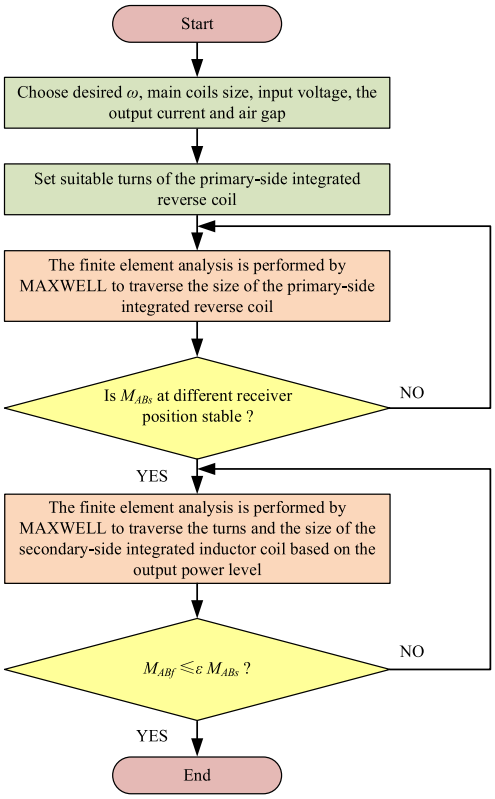

Fig. 5. Design process of the proposed coupler.

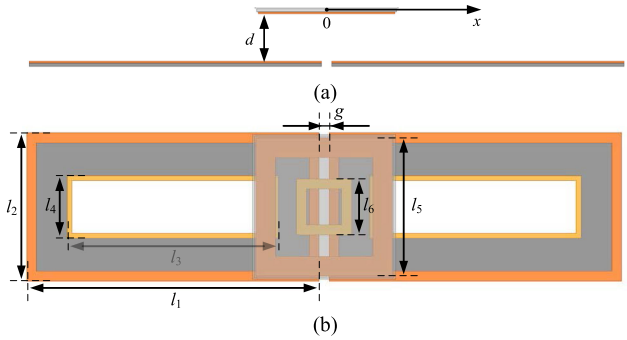

Fig. 6. Structure and dimensions of the magnetic coupler. (a) Front view. (b) Top view.

TABLE I
PARAMETERS OF THE MAGNETIC COUPLER

Parameter	Description	Parameter	Description
l_1	Length of L_{A1} (L_{B1})	l_2	Width of L_{A1} (L_{B1})
l_3	Length of L_{A2} (L_{B2})	l_4	Width of L_{A2} (L_{B2})
l_5	Side length of L_s	l_6	Side length of L_{f3}
n_{w1}	Turns of L_{A1} (L_{B1})	n_{w2}	Turns of L_{A2} (L_{B2})
n_{w3}	Turns of L_s	n_{w4}	Turns of L_{f3}
x	Receiver position	d	Transfer distance
g	Gap distance between adjacent transmitting coils		

should be rationally designed to obtain more stable M_{ABs}. To achieve a ZVS working condition, the secondary-side integrated inductor coil should be designed to obtain $M_{ABf} \leq \varepsilon M_{ABs}$. ε is the index indicating the degree of ZVS. The detailed design is performed in Section III.

III. Design of the Magnetic Coupler

A. Design Process

The crucial idea of the proposed method is to design the integrated reverse coil and integrated inductor coil based on the establishment of the initial magnetic coupler. The design of the integrated reverse coil determines the value of the variable M_{ABs}, which is the key part of the design. According to the guidance of theoretical analysis, the optimized result is obtained by traversed based on the finite element simulation software. The design process of the proposed magnetic coupler is shown in Fig. 5. First, the receiving coil is designed based on the requirements of SAE J2954 WPT3Z3 VA. Furthermore, the transmitting coils are designed comprehensively considering coupling coefficient k and the practical application. Second, under the main coils determined, the primary-side integrated reverse coils are designed to obtain stable M_{ABs} at different receiver positions. Third, based on the transmitting coils with integrated reverse coils, the secondary-side integrated inductor coil is designed to ensure $M_{ABf} \leq \varepsilon M_{ABs}$ at different receiver positions. Finally, based on the simulation design of the main coupling coils and the integrated coils, a magnetic coupler model is constructed in Maxwell to obtain the system parameters.

The whole system structure modeled using Maxwell is shown in Fig. 6. The parameters describing the coupler dimensions are given in Table I. A typical example of a magnetic coupler suitable for 4.5-kW power level is used to explain the design method in this article.

B. Design of the Magnetic Coupler

1) Design of Initial Parameters: The structure of the receiver is designed based on the SAE J2954 WPT3Z3 VA standard. The size of the receiving coil is designed as "400 mm $*$ 400 mm $*$ 5 mm." The turns n_{w3} is designed as 10. The ferrite plate

$$\begin{bmatrix} 0 & j\omega L_{f1} & 0 & 0 & 0 & 0 \\ j\omega L_{f1} & j\omega(L_A - L_{f1}) & 0 & j\omega M_{AB} & -j\omega M_{As} & -j\omega M_{Af} \\ 0 & 0 & 0 & j\omega L_{f2} & 0 & 0 \\ 0 & j\omega M_{AB} & j\omega L_{f2} & j\omega(L_B - L_{f2}) & -j\omega M_{Bs} & -j\omega M_{Bf} \\ 0 & -j\omega M_{As} & 0 & -j\omega M_{Bs} & 0 & j\omega L_{se} \\ 0 & -j\omega M_{Af} & 0 & -j\omega M_{Bf} & j\omega L_{se} & R_e \end{bmatrix} \cdot \begin{bmatrix} \dot{I}_1 \\ \dot{I}_A \\ \dot{I}_2 \\ \dot{I}_B \\ \dot{I}_s \\ \dot{I}_3 \end{bmatrix} = \begin{bmatrix} \dot{U}_{\text{in}} \\ 0 \\ \dot{U}_{\text{in}} \\ 0 \\ 0 \\ 0 \end{bmatrix} \tag{5}$$

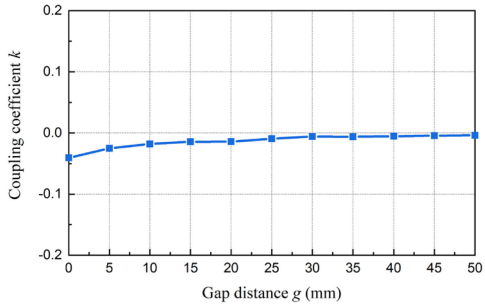

Fig. 7. Relationship between coupling coefficient k and gap distance g.

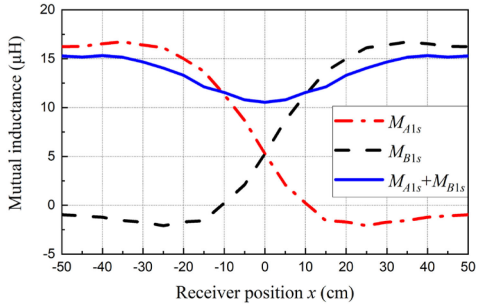

Fig. 8. Variation curves of the main mutual inductance at different receiver positions.

and aluminum shield are used for magnetic field enhancement and electromagnetic shielding, respectively. The size of the secondary-side ferrite board is "400 mm $*$ 400 mm $*$ 10 mm." The size of the aluminum shield is "420 mm $*$ 420 mm $*$ 5 mm." The transfer distance is $d = 150$ mm.

Generally, the coupling coefficient and cost are two primary indicators for designing the main magnetic coupler. In the EVDWC system, the coupling coefficient k is closely related to the power transferability. For a certain length of the road, transmitting coils with shorter lengths require more resonance compensation networks, magnetic cores, and Litz-wires featuring high cost. A typical example of the transmitting coil is designed to construct the initial magnetic coupler, fully considering the length of the EV, cost, magnetic leakage, and coupling coefficient. In this case, the size of the transmitting coils is designed as "900 mm $*$ 450 mm $*$ 5 mm." The turns n_{w1} is designed as 6.

In the EVDWC system, the cross-coupling between two adjacent transmitting coils will cause the activated coils affected by nearby inactive coils. Also, excessive cross-coupling will make it hard to configure the series resonance compensation capacitor in practical applications. A greater gap distance means a greater drop in mutual inductance, which leads to more fluctuation in output power. To avoid excessive cross-coupling, the gap distance g between the two adjacent transmitting coils should be optimized. The relationship between coupling coefficient k and gap distance g is shown in Fig. 7. The result shows that after the gap distance reaches 30 mm, the value of k is negligible and decreases slowly. Therefore, the gap distance g is set to 30 mm.

2) Design of $\mathrm{M_{ABs}}$*:* The variation curves of mutual inductance at different receiver positions are shown in Fig. 8. M_{A1s} and M_{B1s}, respectively, represent the mutual inductance between the receiving coil and two adjacent transmitting coils. Their sum reflects the total coupling of power transmission. The result shows that the main coupling mutual inductance has a severe drop during the transition of transmitting coils, which will lead to the output power fluctuation.

Integrated reverse coils are added to improve the coupling performance between the transmitting coils and the receiving coil. The coupling characteristics of the integrated reverse coils and the receiving coil are expected to be approximately the same as those between the transmitting coils and receiving coil. In this way, the equivalent mutual inductance obtained by the superposition of the two couplings can be sufficiently stable for power transmission.

According to Neumann formula, the mutual inductance between a transmitting coil and a receiving coil can be expressed as

$$M_c = \frac{\mu_0 N_a N_b}{4\pi} \oint_{l_b} \oint_{l_a} \frac{d\vec{l_a} d\vec{l_b}}{r_{ab}} \tag{12}$$

where N_a, N_b, $d\vec{l_a}, d\vec{l_b}$ are the coil turns, the infinitesimal of transmitting coil and receiving coil respectively. r_{ab} is the distance between $d\vec{l_a}$and $d\vec{l_b}$. μ_0 is the magnetic permeability of the vacuum.

According to (12), when the receiving coil is fixed, the mutual inductance is proportional to the turns of the transmitting coil. Based on this, the relationship between the turns of the initial transmitting coil and the turns of the integrated reverse coil is constrained by the following two points. First, the turns n_{w2} should be less than n_{w1} so that the mutual inductance difference is positive, which ensures the forward transmission of power. Second, the ratio of n_{w2} and n_{w1} determines the magnitude of the mutual inductance difference used for power transmission, which should be selected according to the power level. In the 4.5-kW power level prototype, the turns n_{w2} is designed as 3.

The schematic diagram of the coupling coils at the transition center position is shown in Fig. 9. The integrated reverse coil is designed inside the transmitting coil, and they are center-symmetrical. The corresponding parameters are marked in Fig. 9(b). Suppose that the current through the integrated reverse coil is I. l_{p1} and l_{p2} are the short sides of the integrated reverse coil. l_{s1} and l_{s2} are the two sides of the receiving coil. The side length of the receiving coil is q. The length and width of the integrated reverse coil are l_r and w_r, respectively. r is the distance from point p to l_{p2}. r_1 and r_2 are the distances from l_{p2} to l_{s1} and l_{s2}, respectively. In the transition position, the current through l_{p2} brings a negative effect, which is the main reason for the drop in mutual inductance. Therefore, through the Newman formula, the mutual inductance between l_{p2} and the receiving coil is calculated as the theoretical basis for the design.

The magnetic field intensity generated by l_{p2} at point p is expressed as

$$\vec{B} = \frac{\mu_0 I \vec{e}_\alpha}{4\pi r} \left[\cos\theta_1 + \cos\left(\tan^{-1} \frac{r}{w_r - r\cot\theta_1} \right) \right]. \tag{13}$$

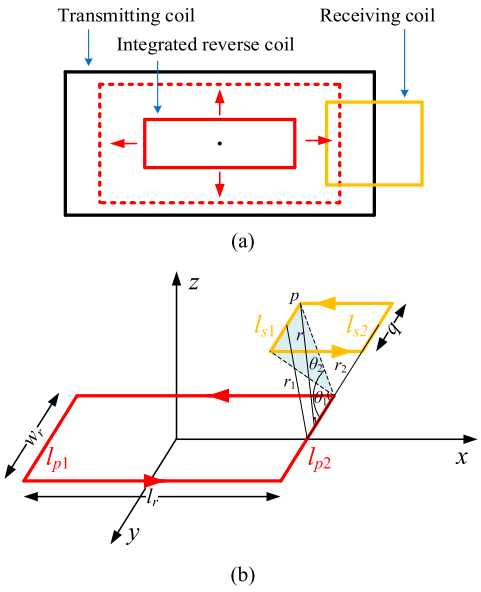

Fig. 9. Schematic diagram of the coupling coils at the transition center position. (a) Top view. (b) Three-dimensional view.

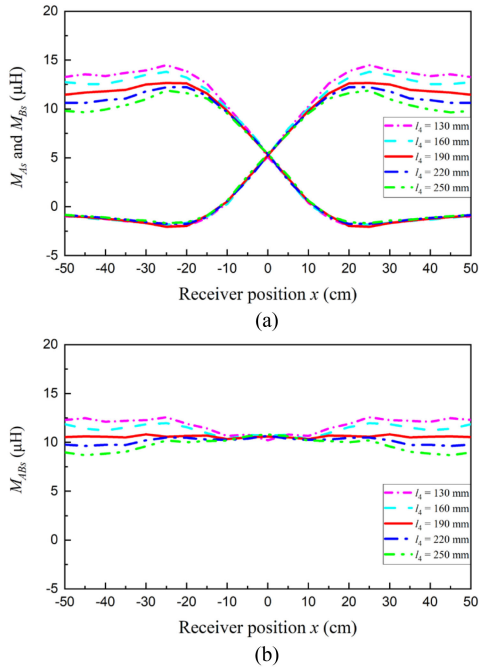

Fig. 10. Variation curves of the mutual inductance at different receiver positions with integrated reverse coils in different widths. (a) Mutual inductance differences between two sets of adjacent primary-side coils and receiving coil. (b) Total equivalent mutual inductance.

Furthermore, the magnetic flux generated from l_{p2} to the receiving coil is calculated as

$$\Phi = -\frac{\mu_0 I q \Delta r}{4\pi r \Delta\theta} \int_{\theta_1}^{\theta_2} \left[\cos\theta + \cos\left(\tan^{-1}\frac{r}{w_r - r\cot\theta}\right)\right] d\theta \tag{14}$$

where $\Delta r = r_2 - r_1$ and $\Delta\theta = \theta_2 - \theta_1$.

The mutual inductance between l_{p2} and the receiving coil is

$$M_{p2} = -\frac{\mu_0 q \Delta r}{4\pi r \Delta\theta} \int_{\theta_1}^{\theta_2} \left[\cos\theta + \cos\left(\tan^{-1}\frac{r}{w_r - r\cot\theta}\right)\right] d\theta. \tag{15}$$

With different lengths and widths, the mutual inductance characteristics at the transition center position could be summarized based on (15). On the one hand, Δr is independent of w_r, and $\Delta\theta$ is approximately unaffected by w_r. When l_r is fixed, the mutual inductance is approximately independent of W. On the other hand, $\Delta\theta$ is approximately unaffected by l_r while Δr decreases as l_r increases. A larger l_r means a bigger M_{p2} under w_r fixed, which makes the negative influence smaller. Therefore, the total coupling mutual inductance at the transition center position is approximately unaffected by w_r but negatively correlated with l_r.

Based on the qualitative characteristics analysis of mutual inductance at the transition position in the EVDWC system revealed by the equations, the design process of the integrated reverse coil is further performed through finite-element simulation. Under the guidance of qualitative analysis, to achieve the stability of M_{ABs}, the design of the integrated reverse coil is optimized in width according to a certain length. The length of the integrated reverse coil is designed as 650 mm. It should be noted that the length of the integrated reverse coil is not unique under the determined initial outer transmitting coil size. Furthermore, there is always a design value of the optimal width under each certain length.

The variation curves of the mutual inductance at different receiver positions with integrated reverse coils in different widths are shown in Fig. 10. Fig. 10(a) shows that after adding integrated reverse coils with different widths, the mutual inductance differences between two sets of adjacent primary-side coils and receiving coil have a certain change rule. At the transition center position, M_{As} and M_{Bs} are independent of width. From the transition center position to the power stable position, the change at the coupling end gradually increases until it stabilizes. This is consistent with the analysis in (15). Fig. 10(b) shows that the fluctuation characteristics of the total equivalent mutual inductance are related to the width, and there exists an optimal value. When the width is 190 mm, the fluctuation of the mutual inductance M_{ABs} in the entire range is within $\pm$ 2%. The size of the integrated reverse coil is designed as "650 mm $*$ 190 mm $*$ 5 mm". Further based on (8), the output power fluctuation is maintained within $\pm$4% in the entire moving range. Therefore, the power fluctuation during the transition of transmitting coils is suppressed effectively.

3) Design of $\mathrm{M_{ABf}}$*:* After designing the integrated reverse coil, the output power fluctuation characteristics have been improved due to the stable mutual inductance difference. The integrated inductor coil on the secondary side needs further design to optimize the ZVS condition. Under the commonly used control strategy of 50% duty cycle, the ZVS working condition is closely related to the phase angle α of the inverter output voltage and current. Specifically, after designing the inductance value according to the output power requirement, the degree of inductance deviation under the ZVS condition is further verified.

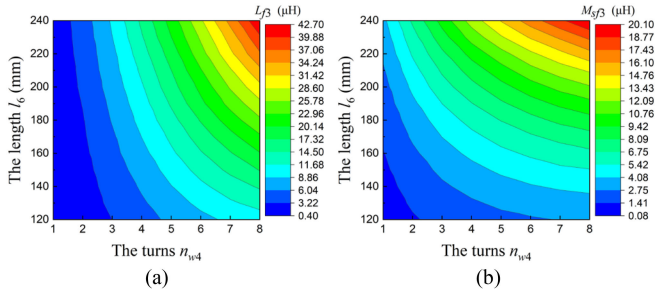

Fig. 11. Analysis of the secondary-side integrated inductor coil parameters affected by the turns *nw*4 and length *l*6. (a) Self-inductance *Lf*3. (b) Mutual inductance *Msf*3.

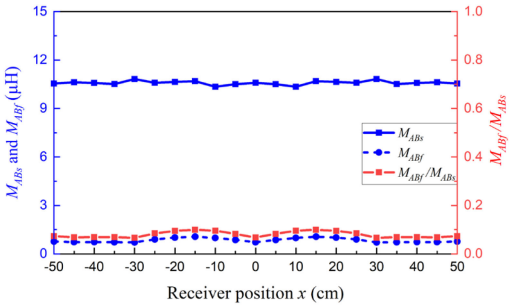

Fig. 12. Variation of *MABs*, *MABf* and *MABf* /*MABs* at different receiver positions.

According to (2), the equivalent inductor in the secondary-side resonant network is L_{fe3}, which is the superposition of L_{f3} and M_{sf3}. Therefore, the crucial design of the secondary-side integrated inductor coil lies in the requirements of L_{f3} and M_{sf3}. Taking n_{w4} and l_6 as variables, the temperature contour maps of L_{f3} and M_{sf3} are obtained by the traversal method, as shown in Fig. 11. Under the same parameter configuration, the internal mutual inductance M_{sf3} and the self-inductance L_{f3} superimpose on behalf of the compensation inductor on the secondary side. The required equivalent self-inductance L_{fe3} can be obtained considering the two parameters comprehensively. In the 4.5-kW power level prototype, the size of the integrated inductor coil is designed as "170 mm $*$ 170 mm $*$5 mm." The turns n_{w4} is designed as 6.

To verify the feasibility of the proposed method, we set the value of ε as 0.1. In this way, $\tan\alpha<0.1$ can achieve, which means that α is less than 5.71°. Compared with 180° of a cycle, it only accounts for 3%. Therefore, the parameter configuration makes the system work in an ideal ZVS condition. Under the designed integrated inductor coil, M_{ABf}, M_{ABs}, and their ratio at different receiver positions are plotted in Fig. 12. The result shows that the ratio of M_{ABf} to M_{ABs} is maintained at a minimum value above 0 and a maximum value within 0.1. It can not only ensure the ZVS working condition but also make the shutdown current not too large.

IV. Experiments

To verify the results of theoretical analysis and design methods, the experimental coils wound according to the design results

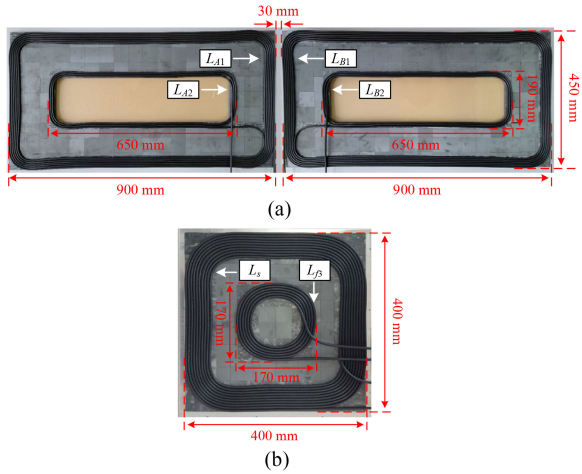

Fig. 13. Prototype of the magnetic coupler with integrated design. (a) Main coils *LA*1, *LB*1 and integrated reverse coils *LA*2, *LB*2. (b) Main coil *Ls* and integrated inductor coil *Lf*3.

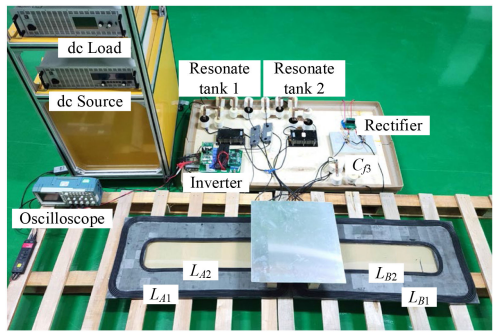

Fig. 14. Prototype of the EVDWC system with integrated design.

in Section III are shown in Fig. 13. The overall experimental prototype is constructed as shown in Fig. 14.

At the input, a dc source and a high-power inverter are used to provide 400 V ac excitation for the resonant circuit. CREE silicon-carbide MOSFETs (C2M0025120D) with 20 mΩ internal resistance are adopted by the inverter to reduce power loss and improve output stability. The voltage rating of these devices is 1200 V, so they can be easily used to adapt the power required by EVs and lay the foundation for future higher power system research. The pulsewidth modulation control signal for the MOSFET is generated by the control chip DSP28335. The output is a fixed frequency of 85 kHz. The two transmitters are the same and connected in parallel. They share a full-bridge inverter. At the output, CREE C3D20060D diodes are used for the rectifier to provide dc current to the EA-CPS-8080 electronic load. The output resistance is set to 20 Ω. The coils are made from 1000-strand AWG 38 Litz-wire. The magnetic material PC95 is used to construct the ferrite board.

The measured parameters of the coupler and the calculated resonance parameters are given in Table II. The theoretical and experimental values of K_1 and M_{ABs} are calculated based on the parameters in Table II. Their values at different receiver positions are shown in Fig. 15. It shows that the variation of

TABLE II
COUPLER MEASURED PARAMETERS AND RESONANCE PARAMETERS

Symbol	Parameters	Quantity
ω	Resonant frequency	85 kHz
L_1	Primary-side compensation inductor	42.0 μH
L_2	Primary-side compensation inductor	42.0 μH
L_{f3}	Secondary-side integrated inductor coil	14.1 μH
L_{A1}	Transmitting coil	84.1 μH
L_{B1}	Transmitting coil	83.7 μH
L_{A2}	Primary-side integrated reverse coil	15.3 μH
L_{B2}	Primary-side integrated reverse coil	15.7 μH
L_s	Receiving coil	93.2 μH
C_1	Primary-side resonance compensation capacitor	152.4 nF
C_2	Primary-side resonance compensation capacitor	152.1 nF
C_{f1}	Primary-side resonance compensation capacitor	184.5 nF
C_{f2}	Primary-side resonance compensation capacitor	184.2 nF
C_{p1}	Primary-side resonance compensation capacitor	44.4 nF
C_{p2}	Primary-side resonance compensation capacitor	44.2 nF
C_s	Secondary-side resonance compensation capacitor	44.5 nF
C_{f3}	Secondary-side resonance compensation capacitor	248.6 nF

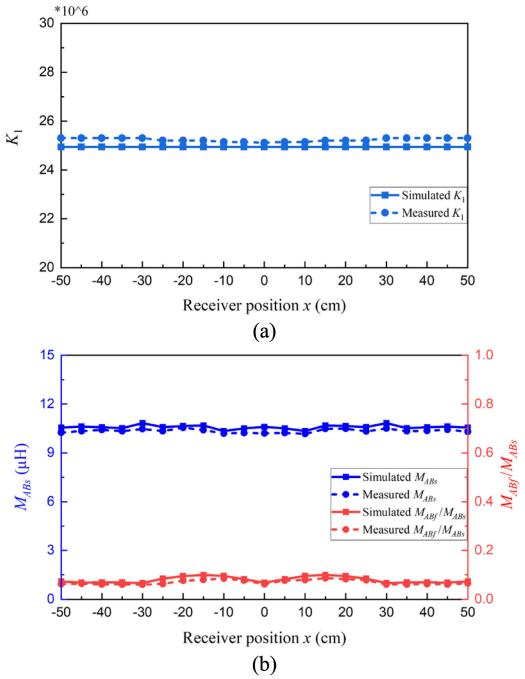

Fig. 15. Variation of crucial design coefficients with the receiver position x under theoretical analysis and experimental measurement. (a) K_1. (b) M_{ABs} and M_{ABf}/M_{ABs}.

the crucial design coefficients K_1, M_{ABs} and M_{ABf}/M_{ABs} are approximately consistent with the theoretical analysis. Simulation and experimental measurement results and characteristics match very well. Therefore, the experimental prototype meets the requirements of the magnetic integrated method proposed in this article for suppressing the power fluctuation.

The inverter output waveforms at different receiver positions are shown in Fig. 16. v_{inv} is the inverter output voltage. $i_{\text{inv}A}$ and $i_{\text{inv}B}$ are the inverter output currents corresponding to the two transmitters. i_{inv} is the superimposed total current of $i_{\text{inv}A}$ and $i_{\text{inv}B}$. The result shows that within a wide range of distance x, the design results guarantee the ZVS working condition under the normal parameter configuration.

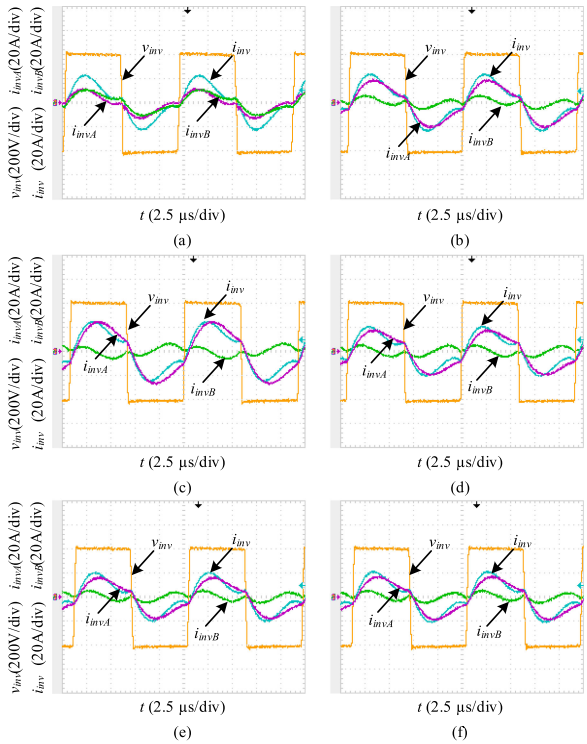

Fig. 16. Steady waveforms of the output voltages and currents of the inverter. (a) $x = 0$ cm. (b) $x = 10$ cm. (c) $x = 20$ cm. (d) $x = 30$ cm. (e) $x = 40$ cm. (f) $x = 50$ cm.

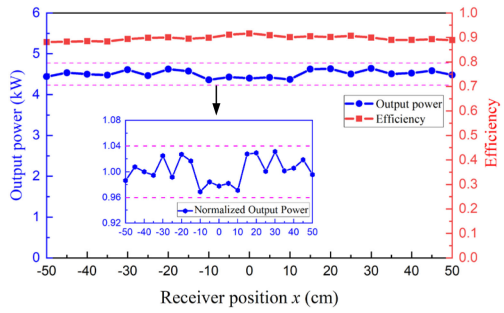

Fig. 17. System output power and efficiency along the transmitting coils.

During the receiver moves above the transmitting coils, the output power and dc–dc efficiency are shown in Fig. 17. The normalized output power obtained with reference to the set value is embedded. The result shows that power fluctuation is suppressed effectively. When the receiver moves from −50 to 50 cm, the output power is between 4.33 and 4.61 kW. The average output power is 4.5 kW, and the power fluctuation is less than ±4% compared with the average power. From dc power supply to dc load, the system efficiency reaches 91.6%.

The method proposed in this article realizes the suppression of power fluctuation during the EV moving. In general, the reverse coil means that more copper will be used at the same power level, resulting in a slight decrease in efficiency at a

single operating point. However, for the overall performance of the EVDWC system under achieving the same power supply across the entire road, the method ingeniously reduces or even eliminates this inherent defect while achieving suppression of power fluctuation.

V. Conclusion

In this article, a magnetic integrated method for the coupler of the EVDWC system including integrated reverse coils and integrated inductor coil to suppress the power fluctuation has been proposed. The integrated reverse coils are connected in series with the transmitting coils, and the integrated inductor coil is in the *LCC* resonance compensation inside the receiving coil. The problem of suppressing power fluctuation is transformed into designing a stable equivalent mutual inductance between the receiving coil and transmitting coils on the road. Two advantages are unveiled through theoretical analysis of system working characteristics: the original single mutual inductance is replaced by the mutual inductance difference between the two reverse series transmitting coils and the receiving coil to determine the power transmission, which suppresses output power fluctuation; the secondary-side integrated inductor coil replaces the external bulky compensation inductor in the *LCC* resonance compensation network and additionally makes the total input impedance of the system appear slightly inductive, which is beneficial for the inverter to work in the ZVS condition. The structures of integrated reverse coils and integrated inductor coil are optimized based on the initial magnetic coupler, and the corresponding design rules are given. A 4.5-kW prototype has been built to verify the theoretical analysis and design method. Experiments show that the proposed magnetic integrated method lowers the level of power fluctuation to less than $\pm 4\%$. The system efficiency from dc source to dc load reaches 91.6%.

References

[1] S. Jeong, Y. J. Jang, and D. Kum, "Economic analysis of the dynamic charging electric vehicle," *IEEE Trans. Power Electron.*, vol. 30, no. 11, pp. 6368–6377, Nov. 2015.

[2] S. Chopra and P. Bauer, "Driving range extension of EV with on-road contactless power transfer—A case study," *IEEE Trans. Ind. Electron.*, vol. 60, no. 1, pp. 329–338, Jan. 2013.

[3] C. C. Mi, G. Buja, S. Y. Choi, and C. T. Rim, "Modern advances in wireless power transfer systems for roadway powered electric vehicles," *IEEE Trans. Ind. Electron.*, vol. 63, no. 10, pp. 6533–6545, Oct. 2016.

[4] K. Lee, Z. Pantic, and S. M. Lukic, "Reflexive field containment in dynamic inductive power transfer systems," *IEEE Trans. Power Electron.*, vol. 29, no. 9, pp. 4592–4602, Sep. 2014.

[5] J. M. Miller *et al.*, "Demonstrating dynamic wireless charging of an electric vehicle: The benefit of electrochemical capacitor smoothing," *IEEE Power Electron. Mag.*, vol. 1, no. 1, pp. 12–24, Mar. 2014.

[6] F. Lu, H. Zhang, H. Hofmann, and C. C. Mi, "A dynamic charging system with reduced output power pulsation for electric vehicles," *IEEE Trans. Ind. Electron.*, vol. 63, no. 10, pp. 6580–6590, Oct. 2016.

[7] X. Zhang, Z. Yuan, Q. Yang, Y. Li, J. Zhu, and Y. Li, "Coil design and efficiency analysis for dynamic wireless charging system for electric vehicles," *IEEE Trans. Magn.*, vol. 52, no. 7, pp. 1–4, Jul. 2016.

[8] Y. Li *et al.*, "A new coil structure and its optimization design with constant output voltage and constant output current for electric vehicle dynamic wireless charging," *IEEE Trans. Ind. Informat.*, vol. 15, no. 9, pp. 5244–5256, Sep. 2019.

[9] H. Li, Y. Liu, K. Zhou, Z. He, W. Li, and R. Mai, "Uniform power IPT system with three-phase transmitter and bipolar receiver for dynamic charging," *IEEE Trans. Power Electron.*, vol. 34, no. 3, pp. 2013–2017, Mar. 2019.

[10] H. Hu *et al.*, "Constant maximum power control for dynamic wireless power transmission system," in *Proc. IEEE PELS Workshop Emerg. Technol., Wireless Power Transf.*, May 2017, pp. 295–299.

[11] C. Wang, C. Zhu, K. Song, G. Wei, S. Dong, and R. G. Lu, "Primary-side control method in two-transmitter inductive wireless power transfer systems for dynamic wireless charging applications," in *Proc. IEEE PELS Workshop Emerg. Technol., Wireless Power Transf.*, 2017, pp. 1–6.

[12] H. Zhu, B. Zhang, and L. Wu, "Output power stabilization for wireless power transfer system employing primary-side-only control," *IEEE Access*, vol. 8, pp. 63735–63747, 2020.

[13] V. -B. Vu, M. Dahidah, V. Pickert, and V.-T. Phan, "A high-power multi-phase wireless dynamic charging system with low output power pulsation for electric vehicles," *IEEE J. Emerg. Sel. Topics Power Electron.*, vol. 8, no. 4, pp. 3592–3608, Dec. 2020.

[14] J. Zhao, T. Cai, S. Duan, H. Feng, C. Chen, and X. Zhang, "A general design method of primary compensation network for dynamic WPT system maintaining stable transmission power," *IEEE Trans. Power Electron.*, vol. 31, no. 12, pp. 8343–8358, Dec. 2016.

[15] H. Feng, T. Cai, S. Duan, J. Zhao, X. Zhang, and C. Chen, "An LCC-compensated resonant converter optimized for robust reaction to large coupling variation in dynamic wireless power transfer," *IEEE Trans. Ind. Electron.*, vol. 63, no. 10, pp. 6591–6601, Oct. 2016.

[16] W. Lee, W. Son, K. Oh, and J. Yu, "Contactless energy transfer systems using antiparallel resonant loops," *IEEE Trans. Ind. Electron.*, vol. 60, no. 1, pp. 350–359, Jan. 2013.

[17] W. Lee, K. Oh, and J. Yu, "Distance-insensitive wireless power transfer and near-field communication using a current-controlled loop with a loaded capacitance," *IEEE Trans. Antennas Propag.*, vol. 62, no. 2, pp. 936–940, Feb. 2014.

[18] W. Lee, K. Oh, and J. Yu, "Field analysis and measurement of antiparallel resonant loop for wireless charging," *IEEE Antennas Wireless Propag. Lett.*, vol. 14, pp. 1459–1462, 2015.

[19] S. Wang, Z. Hu, C. Rong, C. Lu, J. Chen, and M. Liu, "Planar multiple-antiparallel square transmitter for position-insensitive wireless power transfer," *IEEE Antennas Wireless Propag. Lett.*, vol. 17, no. 2, pp. 188–192, Feb. 2018.

[20] J. Kim, H. C. Son, and Y. J. Park, "Multi-loop coil supporting uniform mutual inductances for free-positioning WPT," *Electron. Lett.*, vol. 49, no. 6, pp. 417–419, Mar. 2013.

[21] Y. Chen, R. Mai, Y. Zhang, M. Li, and Z. He, "Improving misalignment tolerance for IPT system using a third-coil," *IEEE Trans. Power Electron.*, vol. 34, no. 4, pp. 3009–3013, Apr. 2019.

[22] Y. Zhang, S. Chen, X. Li, L. Zhang, and Y. Tang, "A design methodology of a free positioning none-overlapping wireless charging system for consumer electronics with a limited parameter variation," in *Proc. IEEE Energy Convers. Congr. Expo.*, 2020, pp. 471–476.

[23] Z. Dong, X. Li, S. Liu, Z. Xu, and L. Yang, "A novel all-direction antimisalignment wireless power transfer system designed by truncated region eigenfunction expansion method," *IEEE Trans. Power Electron.*, vol. 36, no. 11, pp. 12456–12467, Nov. 2021.

[24] Y. Zhang, S. Chen, X. Li, and Y. Tang, "Design methodology of free-positioning nonoverlapping wireless charging for consumer electronics based on antiparallel windings," *IEEE Trans. Ind. Electron.*, vol. 69, no. 1, pp. 825–834, Jan. 2022.

[25] F. Lu, H. Zhang, H. Hofmann, W. Su, and C. C. Mi, "A dual-coupled LCC-compensated IPT system with a compact magnetic coupler," *IEEE Trans. Power Electron.*, vol. 33, no. 7, pp. 6391–6402, Jul. 2018.

[26] L. Zhao, D. J. Thrimawithana, U. K. Madawala, A. P. Hu, and C. C. Mi, "A misalignment-tolerant series-hybrid wireless EV charging system with integrated magnetics," *IEEE Trans. Power Electron.*, vol. 34, no. 2, pp. 1276–1285, Feb. 2019.

[27] K. Shi, C. Tang, H. Long, X. Lv, Z. Wang, and X. Li, "Power fluctuation suppression method for EV dynamic wireless charging system based on integrated magnetic coupler," *IEEE Trans. Power Electron.*, vol. 37, no. 1, pp. 1118–1131, Jan. 2022.

[28] S. Li, W. Li, J. Deng, T. D. Nguyen, and C. C. Mi, "A double-sided LCC compensation network and its tuning method for wireless power transfer," *IEEE Trans. Veh. Technol.*, vol. 64, no. 6, pp. 2261–2273, Jun. 2015.

[29] Q. Zhu, L. Wang, Y. Guo, C. Liao, and F. Li, "Applying LCC compensation network to dynamic wireless EV charging system," *IEEE Trans. Ind. Electron.*, vol. 63, no. 10, pp. 6557–6567, Oct. 2016.

Ke Shi received the B.S. degree in 2016 from the College of Automation, Chongqing University, Chongqing, China, where he is currently working toward the Ph.D. degree in control theory and control engineering.

His current research interests include modeling and control of wireless power transfer and power electronics, dynamic wireless charging systems, and integrated magnetic coupler.

Chunsen Tang (Member, IEEE) received the B.S. and Ph.D. degrees from the College of Automation, Chongqing University, Chongqing, China, in 2004 and 2009, respectively.

In 2008, he was a Research Fellow with the Department of Electrical and Computer Engineering, The University of Auckland, Auckland, New Zealand. In 2009, he was with the College of Automation, Chongqing University, Chongqing, China, where he is currently a Professor. His current research interests include nonlinear modeling and analysis, intelligent control, and wireless power transfer.

Zhihui Wang (Member, IEEE) received the B.S. and M.S. degrees in automation, and the Ph.D. degree in control theory and control engineering from the College of Automation, Chongqing University, Chongqing, China, in 2003, 2006, and 2009, respectively.

He is currently a Professor with the College of Automation, Chongqing University. His current research interests include both fundamental investigations and practical engineering applications in efficient high-power converters and wireless power supply.

Xiaofei Li (Member, IEEE) received the B.S. and Ph.D. degrees from Chongqing University, China, in 2013 and 2018, respectively.

He is currently a Lecturer with the College of Automation, Chongqing University. His current research interests include modeling and control of wireless power transfer and power electronics.

Yuanzhao Zhou received the B.S. degree in 2019 from the College of Automation, Chongqing University, Chongqing, China, where he is currently working toward the M.S. degree in control engineering.

His current research interests include modeling and control of wireless power and power electronics, the design of dynamic wireless charging systems.

Yingjun Fei received the B.S. degree in 2019 from the College of Automation, Chongqing University, Chongqing, China, where he is currently working toward the Ph.D. degree in control theory and control engineering with the College of Automation.

His current research interests include wireless power transfer.